Volume 1 | Number 1 | Jan 2013 | Pages 1–100

Green Chemistry

Cutting-edge research for a greener sustainable future

www.rsc.org/greenchem

Stille couplings in water @RT

ROYAL SOCIETY OF CHEMISTRY

ROYAL SOCIETY OF CHEMISTRY

www.rsc.org/greenchem

Journal Name

COMMUNICATION

Hybrid Wood Materials with Improved Fire Retardance by Bio-inspired Mineralisation on Nano- and Submicron Level

Vivian Merk[a], Munish Chanana[a,b*], Tobias Keplinger[a], Sabyasachi Gaan[c], Ingo Burgert[a*]

Inspired by natural matrix-mediated biomineralisation, we present an artificial calcification approach for wood, which predominately targets the hardly accessible nanoporous cell wall structure rather than the micron-sized void system of the cell lumina. $CaCO_3$ can be deposited with this method deep in the wood structure. Mineralisation of the wood cell wall architecture with $CaCO_3$ offers a green alternative to conventional fire-retardant systems.

The hierarchical structure of plants provides an utilisable nano-and microstructural skeleton at the cell and cell wall level to develop advanced biocomposites with novel material properties. The wood cell wall consists of stiff paracrystalline cellulose nanofibrils which are oriented in a parallel fashion and are embedded in the amorphous matrix components such as hemicelluloses and lignin [1] [2]. This sustainable biocomposite, well known for its excellent mechanical performance [2], has great potential for wider utilisation, given that a better control of functionalisation processes of the intrinsic hierarchical wood structure is achieved. Although being strong and rigid, the cell wall can be regarded as a compact skeleton since it possesses small nanopores between the cellulose fibrils.

In particular, a hybrid material which consolidates the stiff secondary cell wall of wood with a mineral phase at the nanostructural level can result in a highly desirable material combination [3] [4] [5]. A particularly promising but also challenging candidate that could be united with the wood cell wall skeleton to form an advanced and eco-friendly hybrid material for large-scale applications is calcium carbonate ($CaCO_3$).

The insertion of $CaCO_3$ in the wood scaffold is inspired by nature's invention to increase the durability and hardness and reduce the water uptake of the exoskeleton of various species. Screening $CaCO_3$ incidence in nature, it can be noted that it is the most abundant biomineral in corals, pearls, mollusk shells, egg shells and crustacean skeletons [3] [4] [5], whereas calcification occurs rarely in plant cell walls [6]. Generally, plants mineralise their tissues for the end of ion storage and homeostasis in response to unstable calcium levels in the environment [7] [8]. $CaCO_3$ is excreted in reef-building coralline algae [9], wood (vacuoles and cell walls) of oxalogenic trees [10], specialised idioblast cells in leaves of mulberry trees (*Morus alba*) [11] or as amorphous $CaCO_3$ cystoliths in leaves of certain angiosperms [8] [12]. Amorphous calcium carbonate (ACC) has been detected in living organisms either as transient phase or stabilised by additional ions, organic macromolecules or proteins [13] [14] [15].

There have been various approaches to chemically modify or functionalise the native cell wall [16] [17] [18] [19]. However, its impregnation is highly challenging and only a few studies could prove a relatively cell wall specific treatment, in particular with organic or silicon compounds, which indeed resulted in improved material properties [16] [17] [18] [19]. A few approaches have been reported, where $CaCO_3$ has been synthesised in wood using aqueous salt solutions [20], supercritical carbon dioxide [21] or calcium di(methylate) and carbon dioxide [22]. Ionisable surface groups of cellulose [23] and other carbohydrates [24] have been considered as nucleation sites for $CaCO_3$ crystallisation. However, a systematic and eco-friendly modification of the wood cell walls with $CaCO_3$ in aqueous solution at ambient temperature has not been achieved so far. Hence, in this study we investigate an one-pot chemical strategy for the artificial calcification of wood cell walls reminiscent of common biomineralisation pathways in nature [5] [1] [25].

In view of practical applications, our aim is improving wood in one of its major shortcomings, namely the high flammability [26] while retaining natural attributes such as high porosity and low density.

Cellulose pyrolysis (i.e. thermal decomposition) accounts for the major heat release in the combustion of wood, involving flaming combustion of volatiles in the gas phase as well decomposition of char by smoldering or glowing combustion [27] [21]. Classical flame-retardant systems (e. g. ammonium phosphate- [28], boron- [29], silica- [30], or sulphur-based [31] flame retardants) influence pyrolysis processes chemically by accelerating dehydration and carbonisation, inhibiting the production of flammable volatile gases or fostering the formation of insulating coatings or char layers [32].

However, many of these fire-retardant formulations present serious environmental and safety hazards due to the release of toxic or carcinogenic compounds during accidental fires, processing, recycling and usage [33]. Halogen-based fire-retardants, for instance, release large amounts of corrosive hydrogen halides acting as free radical traps in the flame [26]. In this context, an inert and environmentally benign mineral such as $CaCO_3$ would represent an environmental friendly and "green" alternative to the classical flame retardants. By incorporating $CaCO_3$ in the wood cell wall structure, the thermal stability is improved by a different mechanism, i.e. gases (e. g. water, carbon dioxide) released in the endothermic decomposition of hydrated minerals will dilute and cool down the mixture of flammable pyrolysis gases.

Hence, for the artificial calcification of a wood, in particular of spruce (a softwood) and beech (a hardwood) we adapted a method originally proposed for the synthesis of ACC microparticles in aqueous solutions [34] [35] [36]. This approach consists in the alkaline hydrolysis of dimethyl carbonate precursors in the presence of calcium ions inside the cell wall structure, which is depicted in Figure 1A. Induced by a pH shift, gaseous carbon dioxide evolves *in situ* [34], hence concentration gradients across the bulk sample and a rapid mineral precipitation in the wood lumina are circumvented to a great extent. Due to the addition of excess sodium hydroxide solution a quantitative hydrolysis of the precursor dimethyl carbonate can be achieved, throughout the wood samples. In this study, wood samples of 2 cm edge length were completely mineralized (Figure 1B). In this process, only water-soluble by-products, namely sodium chloride and methanol, are formed, which do not interfere with the nucleation and growth of $CaCO_3$[35] and can be easily removed by washing and/or drying. In view of process sustainability, common membrane techniques enable the separation of ternary dimethyl carbonate/methanol/water mixtures for the removal of excess unreacted DMC [37].

Figure 1. A: Schematic depiction of the mineralisation of wood by alkaline hydrolysis of dimethyl carbonate in the presence of calcium ions within the wood matrix. B: Photo of unmodified and mineralised spruce and beech samples (2 cm edge length). Light microscopic images of mineralised beech (C) and spruce specimens (D). The scale bars in C and D correspond to 500 μm.

As shown in Figure 1B, the resulting wood/$CaCO_3$ composites and native wood appear very similar macroscopically. Light microscopic images of cross-cut $CaCO_3$/wood composites (**Figure 1**C, D) indicated little calcerous minerals filling up the bigger lumina of hardwood vessels and early softwood tracheids. These results were confirmed *via* scanning electron microscopy (SEM) of the cross-cut $CaCO_3$/wood composites in the backscattered electron mode (**Figure 2**).

In the case of spruce, mineral compounds seem to agglomerate prevailingly along the middle lamellae, primary cell walls and cell corners of vicinal cells where calcium-complexing pectins are abundant [38] [39] [40]. Polyuronates offer as natural negatively-charged polyelectrolytes calcium-binding sites where $CaCO_3$ nucleation is favoured [39] [40]. Electron-rich material (*i.e.* $CaCO_3$) can be observed in the cell walls of beech fibres, within parenchyma cells, as well as spruce latewood tracheids and ray cells (**Figure 2**A,B and **2**D,E respectively) at higher magnifications. Judging from the morphological features, the electron-lucent deposits appear amorphous, although further analytical characterisations of the minerals refer to dried samples due to the necessary sample preparation.
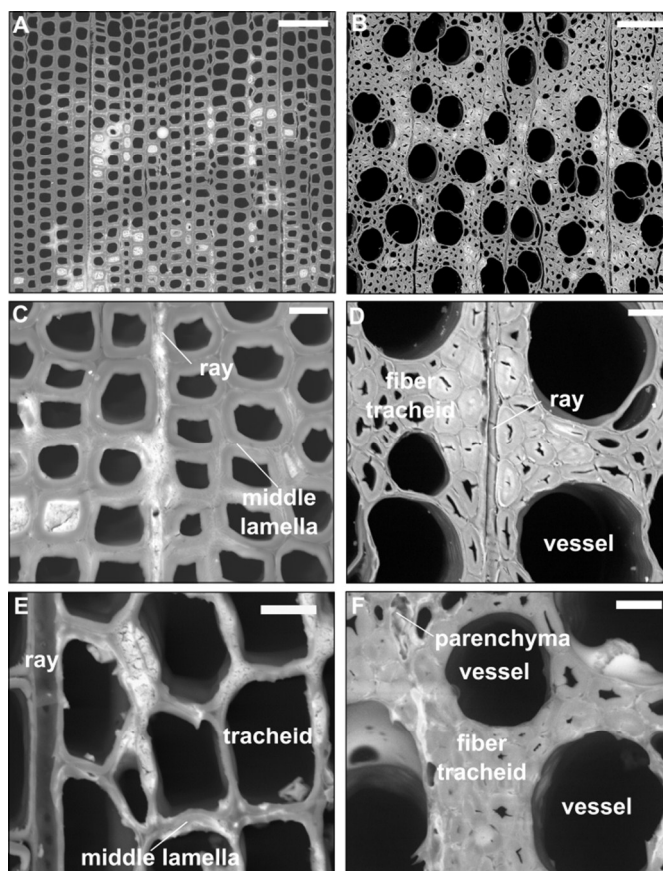

Figure 2. Low-vacuum scanning electron microscopy of microtome cross-sections of spruce (A, C, E) beech (B, D, F) $CaCO_3$ composites prepared at [DMC] = [$CaCl_2$] = 1.5 mol L^{-1} prior to drying. SEM images in the backscattered electron mode give evidence of relatively void lumina and depositions of electron-dense material along middle lamellae and rays, within beech fibres and parenchyma cells. Scale-bars correspond to 500 μm (A, B), 100 μm (C, D) and 20 μm (E, F).

Furthermore, the mineral distribution in the wood bulk was investigated *via* SEM/EDX. The semi-quantitative energy-dispersive X-ray point microanalysis of the CaK_α line brings a further proof of

the presence of calcium-containing mineral incorporated in the wood cell walls of both species, sodium chloride as a side product of the process and unreacted calcium chloride (Figure S12-17). Hence, the predominant mineral deposition takes place in the nano-and submicron-sized pores of the wood cell wall structure. A plausible explanation for this could be the interplay of capillary forces and the evolution of gaseous CO_2. Due to the capillary forces, the liquid phase with the dissolved precursors are imbided into the nano- and submicron pores, whereas due the evolution of CO_2 bubbles, which presumably will gather and grow in the bigger cell voids (i.e cell lumina and vessels), the mineral precipitation in these large pores of wood is hindered. Furthermore, EDX suggests a non-quantitative reaction of $CaCl_2$ and DMC to $CaCO_3$ due to the highly saturated precursor solutions employed in this study. Nonetheless, the highly water-soluble salts NaCl and $CaCl_2$ can be removed by washing in slightly basic water, as verified by XRD (Figure S16-17, SI). For an industrial application as flame-retardant, sodium chloride in addition to $CaCO_3$ is beneficial due to the higher overall mineral content and increased wood humidity (Figure 7, SI).

$CaCO_3$ has been detected in bulk wood by infrared spectroscopy (Figure S1, supporting information) and X-ray powder diffraction (S18, supporting information), but these techniques do not provide insight into the spatial distribution of $CaCO_3$ over the wood cell hierarchy. Using confocal Raman microscopy we investigated the mineralogy and localisation of $CaCO_3$ within the wood tissue in greater detail. The most prominent CO_3^{2-} vibration absorption (v_1) of $CaCO_3$ polymorphs lies in the spectral range of 1089-1069 cm^{-1} [41] [42] partly overlapping with the cellulose bands of wood in the wavenumber area 1090-1105 cm^{-1} [43]. Spectral features allow to discriminate among the possible crystalline $CaCO_3$ polymorphs [41], amorphous and hydrated forms [42] [44]. This is why small and evenly distributed amounts of $CaCO_3$ can hardly be detected by mere peak integration. However, vertex component analysis [45] [46] allows for deconvoluting the hyperspectral dataset. This multivariate method furnishes representative endmember spectra for the most distinct cell wall components, namely aromatic lignin, carbohydrates, water or $CaCO_3$. Colour-coded mappings (Figure 3) reflect the cell wall composition by visualising the similarity between each collected spectrum to the respective endmember spectrum (Figure 3C,F,I). An endmember with an absorption band at 1140-1160 cm^{-1} can be attributed to the aromatic polymer lignin (Figure 3A, B) which is most abundant in cell corners and middle lamellae at the boundary between vicinal cells. Endmembers with peaks at 1095 cm^{-1},
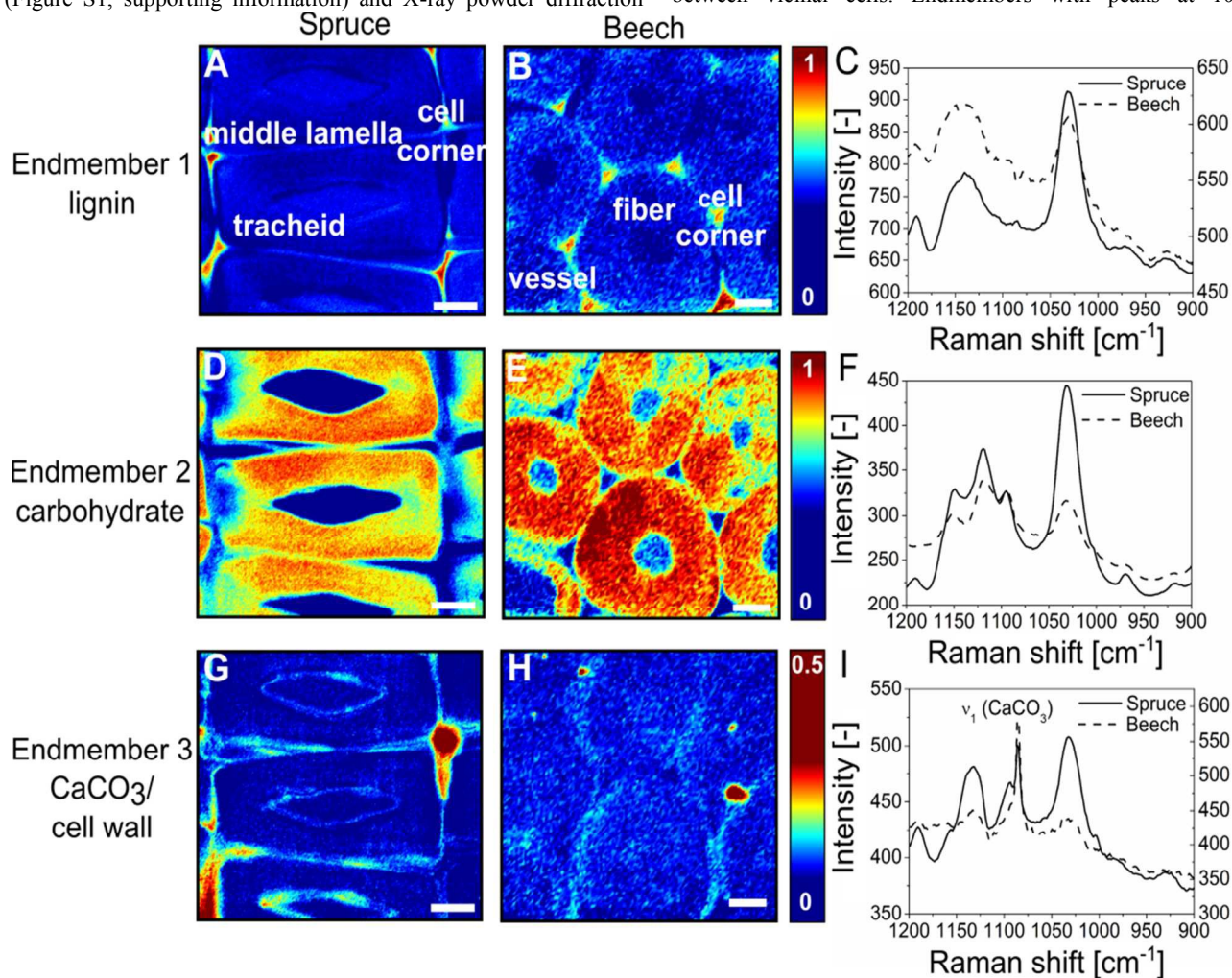
Figure 3. Raman mappings of $CaCO_3$/wood composites prepared at [DMC] = [$CaCl_2$] = 1.0 mol L^{-1} according to VCA analysis showing endmembers of spruce (A, D, G, solid line) and beech (B, E, H, dashed line) in the range |1200-900 cm^{-1}|. Endmember 1 (A, B): Lignin-rich cell corners and middle lamellae (1125-1175 cm^{-1}). Endmember 2 (D, E): Secondary cell wall carbohydrates (1112 cm^{-1}, 1154 cm^{-1}). Endmember 3 (G, H): $CaCO_3$ mineral (1080-1090 cm^{-1}) prevailingly in middle lamellae and cell corners. C, F, I: Endmember spectra for spruce (solid line) and beech (dashed line) in the range |1200-900 cm^{-1}|. The left axes in 3C and 3I refer to spruce, the right axis to beech. Scale-bars in A, D, G correspond to 10 μm and in B, E, H to 5 μm, respectively.

1118 cm^{-1} and 1151 cm^{-1} represent secondary (Figure 3D-F) and primary cell walls (Figure S2d-f, supporting information). The primary cell wall can be discerned by a higher height of the orientation-sensitive cellulose peak at 1095 cm^{-1}. In Figure 3G,H, the strong v_1 (CaCO$_3$) vibration at 1086 cm^{-1} together with cell-wall-sensitive spectral bands indicates the presence of calcite within spruce tracheids (Figure 3A,D,G) and beech fibres (Figure 3B,E,H) predominantly at the boundary between interconnected cells.
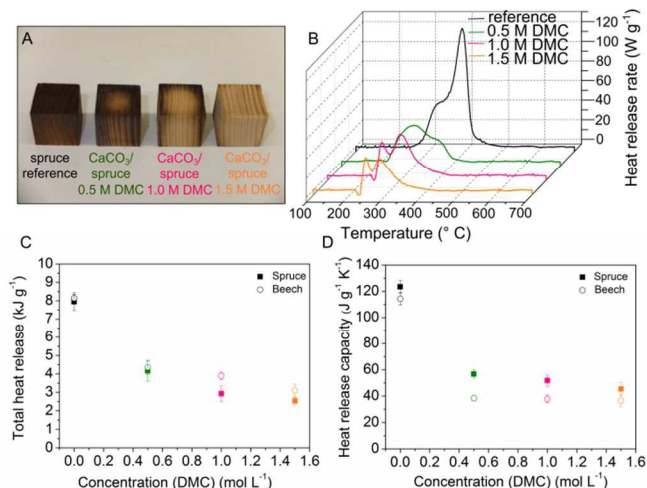
Figure 4. A: Photo of native spruce and spruce/CaCO$_3$ composites after burning in a muffle furnace (20 min, 250° C). B: Typical temperature-dependent heat release rate curves from pyrolysis combustion flow calorimetry (PCFC) of beech samples after base-line correction. The key parameters total heat release (C) and heat release capacity (D) of spruce and beech are plotted as a function of the precursor concentration [DMC] = [CaCl$_2$].

To evaluate the material improvement based on the nanoscale modification, the macroscopic characteristics of the hybrid material are of particular relevance. For instance, hierarchically structured crystalline and amorphous CaCO$_3$ minerals give rise to the superior mechanical properties of chitineous lobster skeletons [47]. Using the mild modification approach of controlled DMC hydrolysis Vilela *et al* reported a higher mechanical performance of CaCO$_3$/cellulose nanocomposite materials compared to native cellulose [48]. In this work we have investigated the fire behaviour of the inorganic/wood composites (in micro-scale) using pyrolysis combustion flow calorimetry (PCFC) and thermogravimetric analysis. It is evident that mineralised spruce (**Figure 4**A) remains physically more intact than untreated spruce after a prolonged heat treatment in a muffle furnace (20 min, 250° C). The complex line shape of the heat release rate curves of PCFC reflects the successive pyrolysis of the wood constituents hemicellulose, cellulose and lignin, as illustrated in **Figure 4**B for beech, was deconvoluted by using a multiple Gaussian fitting technique. HRR curves of spruce timber presented in **Figure S4** (Supporting information) show one dominant heat release rate maximum originating from the exothermic oxidation of aliphatic cellulose units at 350° C [32][27] overlapped by a high-temperature shoulder from lignin degradation present in all measured HRR spectra [49][50]. Beech decomposes by a two-step (second order) process through thermal degradation of hemicelluloses at 270° C followed by cellulose pyrolysis around 350° C [49]. The incorporation of minerals into the wood architecture affects the cellulose thermal decomposition by reducing the formation of volatiles. The fire

properties, namely the total heat of combustion, the heat release capacity and the char residue are significantly improved (**Figure 4**C-D, **Figure S6**).

The net heat of combustion of the CaCO$_3$/wood composites measured by pyrolysis combustion flow calorimetry decreased to approximately a third (32-38 %) compared to unmodified wood (**Figure 4**C). A crucial indicator of fire hazard is the tendency to ignite objects nearby or to maintain flaming combustion. Thus, the potential for fire propagation is mainly assessed by the heat release capacity [51]. Compared to native wood the heat release capacity of the CaCO$_3$/wood composites was found to decrease substantially to 37 % of the original value for spruce and 32 % for beech (**Figure 4**D). Notably, total heat release and heat release capacity values obtained for spruce/CaCO$_3$ composites [DMC] = 1.5 mol L^{-1}) resemble those reported for halogenated high-performance polymers like poly(tetrafluoroethylene), Teflon™ (THR = 3.7 kJ g^{-1}, HRC = 35 J g^{-1} K^{-1} [52]) commonly used as heat-resistant coatings. Since the char yield of the composites is approximately doubled compared to native wood (**Figure S6**) the embedded mineral possibly contributes to the fire-retardant capacity of wood.

Furthermore the incorporated CaCO$_3$ also improves the thermal stability of wood materials. The equilibrium moisture content of the mineralised samples increased as a function of DMC content (**Figure S7**), likely due to residual sodium chloride in the wood composite, as detected by SEM-EDX (Figure S12-17) and XRD (Figure S18). Hence, gases (e. g. water vapour, carbon dioxide) released in the endothermic decomposition of hydrated minerals may have a diluting and cooling effect on the flammable pyrolysis gases. Further, the inorganic matrix diluents also improve the fire performance by fostering the self-insulating char formation of wood and inhibiting heat transfer and smoke evolution [53][54]. CaCO$_3$, as a weak base, might catalyse the pyrolytic decomposition/depolymerisation of cellulose favouring the production of stable char and non-flammable gases over levoglucosan and other tar anhydrosugars [55][56][57]. Additionally, TGA data confirms a lowered decomposition temperature and an increased char formation (**Figures S8-11**) for the treated wood samples.

Conclusions

In conclusion, the insertion of CaCO$_3$ in the wood scaffold is inspired by nature's invention to increase the durability and hardness and reduce the water uptake of the exoskeleton of various species. More importantly, it transfers the principle to a technical level by addressing a severe timber engineering problem. The bio-inspired mineralisation as proposed in the current work highly improves the flame retardancy of wood and hence, considerably expands its reliability in constructions without impairing the intrinsic key benefits of wood arising from its biological nature. The fact that a softwood (spruce) and a hardwood (beech) gave similar results under similar treatment conditions, shows the versatility of the process. We conclude that the specific material combination of wood and CaCO$_3$ results in a hybrid material that has the potential to become one of the key construction materials, because of its improved reliability on top of a renewable nature, positive carbon footprint, eco-friendliness, and excellent mechanical performance in view of a still comparably low density. Above all, the concept of wood-mineral nanocomposites making use of a directed mineralisation in the hierarchical scaffold of the wood material opens new ways to develop a multitude of

advanced hybrid-materials, based on various mineral combinations and a vast diversity of wood species.

Notes and references

[a] Wood Materials Science, Institute for Building Materials (IfB), ETH Zürich, Stefano-Franscini-Platz 3, 8093 Zürich, Switzerland.
Applied Wood Materials Laboratory, EMPA - Swiss Federal Laboratories for Materials Science and Technology, 8600 Dübendorf, Switzerland.
[b] Physical Chemistry II, University of Bayreuth, University of Bayreuth, Universitätstr. 30, 95447 Bayreuth, Germany.
[c] Advanced Fibres, EMPA - Swiss Federal Laboratories for Materials Science and Technology, Lerchenfeldstrasse 5, 9014 St. Gallen, Switzerland.

Electronic Supplementary Information (ESI) available: Experimental section; IR spectra of $CaCO_3$/wood composites; Raman endmember mappings; PCFC heat release curves; sample mass gain; char yield; equilibrium moisture content; TGA curves; TGA derivatives; semi-quantitative EDX analysis of $CaCO_3$/wood composites, X-ray powder diffraction of mineralised spruce. See DOI: 10.1039/c000000x/

1. P. Fratzl and R. Weinkamer, *Progress in Materials Science*, 2007, **52**, 1263-1334.
2. L. Salmen and A. M. Olsson, *Journal of Pulp and Paper Science*, 1998, **24**, 99-103.
3. F. C. Meldrum, *International Materials Reviews*, 2003, **48**, 187-224.
4. S. Weiner and L. Addadi, *Journal of Materials Chemistry*, 1997, **7**, 689-702.
5. S. Weiner and L. Addadi, in *Annual Review of Materials Research, Vol 41*, eds. D. R. Clarke and P. Fratzl, 2011, pp. 21-40.
6. P. F. Arnott HT, in *Biological Calcification: Cellular and molecular aspects*, ed. S. H, North-Holland Amsterdam, 1970.
7. M. A. Webb, *The Plant Cell Online*, 1999, **11**, 751-761.
8. M. G. Taylor, K. Simkiss, G. N. Greaves, M. Okazaki and S. Mann, *Proceedings of the Royal Society B-Biological Sciences*, 1993, **252**, 75-80.
9. T. F. Goreau, *Annals of the New York Academy of Sciences*, 1963, **109**, 127-167.
10. G. Cailleau, O. Braissant and E. P. Verrecchia, *Biogeosciences*, 2011, **8**, 1755-1767.
11. I. Nitta, A. Kida, Y. Fujibayashi, H. Katayama and Y. Sugimura, *Protoplasma*, 2006, **228**, 201-208.
12. A. Gal, V. Brumfeld, S. Weiner, L. Addadi and D. Oron, *Advanced Materials*, 2012, **24**, OP77-OP83.
13. L. Addadi, S. Raz and S. Weiner, *Advanced Materials*, 2003, **15**, 959-970.
14. A. Gal, S. Weiner and L. Addadi, *Journal of the American Chemical Society*, 2010, **132**, 13208-13211.
15. J. Aizenberg, L. Addadi, S. Weiner and G. Lambert, *Advanced Materials*, 1996, **8**, 222-226.
16. S. Kumar, *Wood Fiber Sci.*, 1994, **26**, 270-280.
17. E. Cabane, T. Keplinger, V. Merk, P. Hass and I. Burgert, *ChemSusChem*, 2014, **7**, 1020-1025.
18. M. A. Ermeydan, E. Cabane, P. Hass, J. Koetz and I. Burgert, *Green Chemistry*, 2014, **16**, 3313-3321.
19. C. Mai and H. Militz, *Wood Sci. Technol.*, 2004, **37**, 339-348.
20. C. Y. Wang, C. Y. Liu and J. Li, in *Environment Materials and Environment Management Pts 1-3*, eds. Z. Y. Du and X. B. Sun, Trans Tech Publications Ltd, Stafa-Zurich, 2010, pp. 1712-1715.
21. C. Tsioptsias and C. Panayiotou, *J Mater Sci*, 2011, **46**, 5406-5411.
22. S. Klaithong, D. Van Opdenbosch, C. Zollfrank and J. Plank, *Zeitschrift Fur Naturforschung Section B-a Journal of Chemical Sciences*, 2013, **68**, 533-538.
23. H. Matahwa, V. Ramiah and R. D. Sanderson, *Journal of Crystal Growth*, 2008, **310**, 4561-4569.
24. A. Rao, J. K. Berg, M. Kellermeier and D. Gebauer, *European Journal of Mineralogy*, 2014.
25. J. W. Morse, R. S. Arvidson and A. Lüttge, *Chemical Reviews*, 2007, **107**, 342-381.
26. R. M. Rowell, *Handbook of Wood Chemistry and Wood Composites*, CRC Press, Boca Raton, 2012.
27. Y. Sekiguchi and F. Shafizadeh, *Journal of Applied Polymer Science*, 1984, **29**, 1267-1286.
28. M. Hagen, J. Hereid, M. A. Delichatsios, J. Zhang and D. Bakirtzis, *Fire Safety Journal*, 2009, **44**, 1053-1066.
29. G. Tondi, L. Haurie, S. Wieland, A. Petutschnigg, A. Lacasta and J. Monton, *Fire and Materials*, 2013, n/a-n/a.
30. I. Simkovic, H. Martonova, D. Manikova and O. Grexa, *Journal of Applied Polymer Science*, 2005, **97**, 1948-1952.
31. I. Simkovic, H. Martvonova, D. Manikova and O. Grexa, *Fire and Materials*, 2007, **31**, 137-145.
32. T. Hirata, S. Kawamoto and T. Nishimoto, *Fire and Materials*, 1991, **15**, 27-36.
33. A. R. Horrocks, *Fire retardant materials*, CRC Press Boca Raton, Fla., 2001
34. M. Faatz, F. Gröhn and G. Wegner, *Advanced Materials*, 2004, **16**, 996-1000.
35. M. Faatz, F. Gröhn and G. Wegner, *Materials Science and Engineering: C*, 2005, **25**, 153-159.
36. K. Gorna, M. Hund, M. Vučak, F. Gröhn and G. Wegner, *Materials Science and Engineering: A*, 2008, **477**, 217-225.
37. W. Won, X. Feng and D. Lawless, *Journal of Membrane Science*, 2002, **209**, 493-508.
38. K. H. Caffall and D. Mohnen, *Carbohydrate Research*, 2009, **344**, 1879-1900.
39. G. T. Grant, E. R. Morris, D. A. Rees, P. J. C. Smith and D. Thom, *Febs Letters*, 1973, **32**, 195-198.
40. M. C. Jarvis, *Plant Cell Environ.*, 1984, **7**, 153-164.
41. C. G. Kontoyannis and N. V. Vagenas, *Analyst*, 2000, **125**, 251-255.
42. M. M. Tlili, M. B. Amor, C. Gabrielli, S. Joiret, G. Maurin and P. Rousseau, *Journal of Raman Spectroscopy*, 2002, **33**, 10-16.
43. N. Gierlinger and M. Schwanninger, *Plant Physiology*, 2006, **140**, 1246-1254.
44. L. Brecevic and A. E. Nielsen, *Journal of Crystal Growth*, 1989, **98**, 504-510.

45. J. M. Nascimento and J. M. Bioucas Dias, *Geoscience and Remote Sensing, IEEE Transactions on*, 2005, **43**, 898-910.

46. N. Gierlinger, *Frontiers in Plant Science*, 2014, **5**.

47. H. O. Fabritius, C. Sachs, P. R. Triguero and D. Roobe, *Advanced Materials*, 2009, **21**, 391-400.

48. C. Vilela, C. S. R. Freire, P. A. A. P. Marques, T. Trindade, C. Pascoal Neto and P. Fardim, *Carbohydrate Polymers*, 2010, **79**, 1150-1156.

49. F. Yao, Q. Wu, Y. Lei, W. Guo and Y. Xu, *Polymer Degradation and Stability*, 2008, **93**, 90-98.

50. M. Brebu and C. Vasile, *Cellulose Chemistry and Technology*, 2010, **44**, 353-363.

51. R. E. Lyon and R. N. Walters, *Journal of Analytical and Applied Pyrolysis*, 2004, **71**, 27-46.

52. R. N. Walters and R. E. Lyon, *Journal of Applied Polymer Science*, 2003, **87**, 548-563.

53. P. Hornsby, in *Fire Retardancy of Polymeric Materials, Second Edition*, CRC Press, 2009, pp. 163-185.

54. T. R. Hull, A. Witkowski and L. Hollingbery, *Polymer Degradation and Stability*, 2011, **96**, 1462-1469.

55. F. Shafizadeh, *Journal of Analytical and Applied Pyrolysis*, 1982, **3**, 283-305.

56. C. Di Blasi, A. Galgano and C. Branca, *Industrial & Engineering Chemistry Research*, 2009, **48**, 3359-3369.

57. D. J. Nowakowski and J. M. Jones, *Journal of Analytical and Applied Pyrolysis*, 2008, **83**, 12-25.

TOC Graphic

Sustainable societies require the development of engineered hybrid materials. Bio-inspired mineralization of the wood cell wall architecture with calcium carbonate offers a green alternative to conventional fire-retardant systems.

Vivian Merk, Munish Chanana*, Tobias Keplinger, Sabyasachi Gaan, Ingo Burgert*

Hybrid Wood Materials with Improved Fire Retardance by Bio-inspired Mineralization on Nano- and Submicron Level
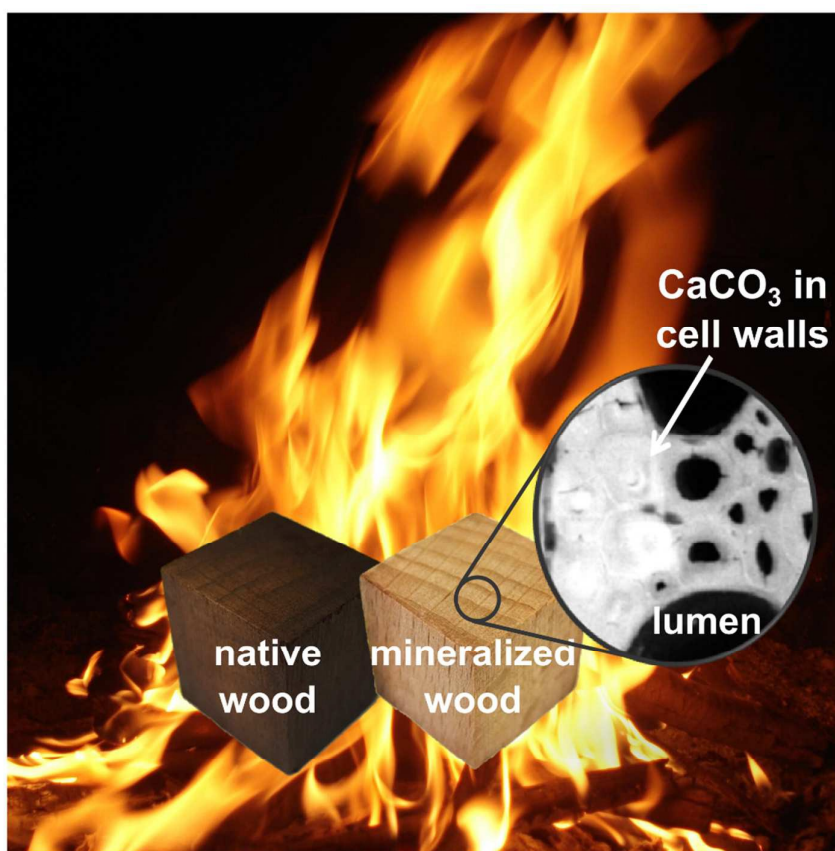
SUPPORTING INFORMATION

Hybrid Wood Materials with Improved Fire Retardance by Bio-inspired Mineralization on Nano- and Submicron Level

Vivian Merk, Munish Chanana*, Tobias Keplinger, Sabyasachi Gaan, Ingo Burgert*

Experimental section

Mineralization of wood: Blocks of Norway spruce (Picea abies) and European beech (Fagus sylvatica) (10 mm or 20 mm edge length) were conditioned at norm climate (65 % relative humidity, 20° C) and dried in a BINDER vacuum oven at 65°C for 48 h. The presented mineralization approach is a facile one-pot process in water at room temperature. Dimethyl carbonate (Sigma Aldrich Reagent Plus, 99 %), calcium chloride dihydrate (Merck, EMSURE ACS Reag. PhEur) and sodium hydroxide (pellets for analysis, Merck, ACS Reag. PhEur) were used without prior purification. Equimolar amounts of dimethyl carbonate and $CaCl_2$ (0.5 mol L^{-1}, 1.0 mol L^{-1}, 1.5 mol L^{-1}) were dissolved in deionized water at ambient temperature and stirred vigorously. The wood samples were incubated for 24 h in the saturated solutions and vacuum-impregnated for several times to allow for in-depth diffusion into the porous wood structure. After initiating the hydrolysis of the organic precursor by adding a 1 M solution of sodium hydroxide until a solution pH ≈ 9 was reached, the wood samples were kept for additional 24 h in the reaction solution. Upon addition of excess sodium hydroxide solution a quantitative hydrolysis of the precursor dimethyl carbonate can be achieved. Finally, the samples were washed with deionized water for 1 h and dried in oven 65°C until weight constancy, in order to remove water, the byproduct methanol (bp: 65°C) and DMC (bp: 90°C) . The mass gain of the samples was determined in the oven-dry state and under norm climate conditions before and after mineralization (see Figure S5, supporting information).

Light microscopy: Cross-cut wood specimens were observed under a Leica M165C stereomicroscope (3.2x objective) coupled to a Basler GigE Vision camera. Images were recorded with a control plugin (PHASE GmbH) for the programme ImageJ 1.47c.

Scanning electron microscopy: Environmental scanning electron microscopy (ESEM) was carried out on a FEI Quanta 600 in the low-vacuum mode (water vapour, 0.53 Torr) driven by 20 kV acceleration voltage using a spot size of 6.0 using a backscattered electron detector. Energy-dispersive X-ray analysis was performed on a FEI Quanta 200 3D scanning electron microscope in the low-vacuum mode (water vapour, 0.53 Torr) driven by 20 kV acceleration voltage using a spot size of 6.0 using a backscattered electron detector.

Raman microscopy: For the Raman measurements 20 μm cross-sections were prepared with a rotary microtome (Leica Ultracut, Germany)), placed on a microscopic slide with a few drops of methanol and sealed with a cover slip and nail polish to avoid evaporation. All Raman spectra were recorded with a confocal Raman-microscope (Renishaw InVia) equipped with a Nd-YAG laser (λ = 532 nm), a 1800 grooves/mm grating and a 100x oil immersion objective (Nikon, NA = 1.4), a step width of 300 nm and an integration time of 0.15 s (spruce) or 0.30 s (beech) due to higher fluorescence. The data were processed with the software Wire 3.4 and single spectra plotted with the program OriginPro 8.1. Additionally, for the extraction of hyperspectral data, the spectral dataset was scanned for cosmic rays and Vertex Component Analysis (VCA) was performed in the spectral range 900-1200 cm^{-1} with the MatLab-based software CytoSpec v. 2.00.01 assuming six endmembers.

Infrared spectroscopy: FT-IR spectra of chopped wood samples were collected with a Tensor 27 spectrometer (Bruker) eqipped with a Pike ATR cell in a spectral range of 4000-350 cm^{-1} with 4 cm^{-1} spectral resolution and averaged over 100 scans. The spectra were recorded and background-corrected with the program OPUS and plotted with OriginPro 8.1.

Pyrolysis combustion flow calorimetry: The heat of combustion of wood-$CaCO_3$ composites and reference wood conditioned to norm climate was determined by oxygen consumption applied to the combustion gases in pyrolysis combustion flow calorimetry (PCFC) (Fire Testing Technology Instrument UK) according to the procedure described in the literature [1] with a pyrolysis temperature of 85−750°C and a 80 % N_2/20 % O_2 gas mixture and operated at a heating rate of β = 1 K s^{-1} and a combustion temperature of 900°C. The PCFC measurements were replicated at least five times for samples of approximately 5 mg. The HRR curves were baseline-corrected and fitted with multiple Gauss curves using the program OriginPro 8.1. Herein, the resulting peak sum (the total heat release) displayed residual values close to 1. The maximum heat release divided by the constant heating rate β = 1 K s^{-1} gives the heat release capacity.

Thermogravimetric analysis: Thermogravimetric analyses of ~10 mg wood specimens were performed using a Q50 TGA (TA instruments) with a heating rate of 20° C min^{-1} in a N_2 atmosphere (60 mL min^{-1} sample purge flow, 40 mL min^{-1} balance purge flow in the 30-1000° C temperature range.

X-ray powder diffraction: XRD spectra were collected from a chopped mineralized spruce sample (~0.25 cm^3) on a Bruker D8 Advance instrument equipped with a copper X-ray source (40 kV voltage, 40 mA current) and a rotating flat disk sample holder using a scan speed of 0.15° min^{-1} in a 2θ = 10-90° range.

Characterization

Infrared spectroscopy
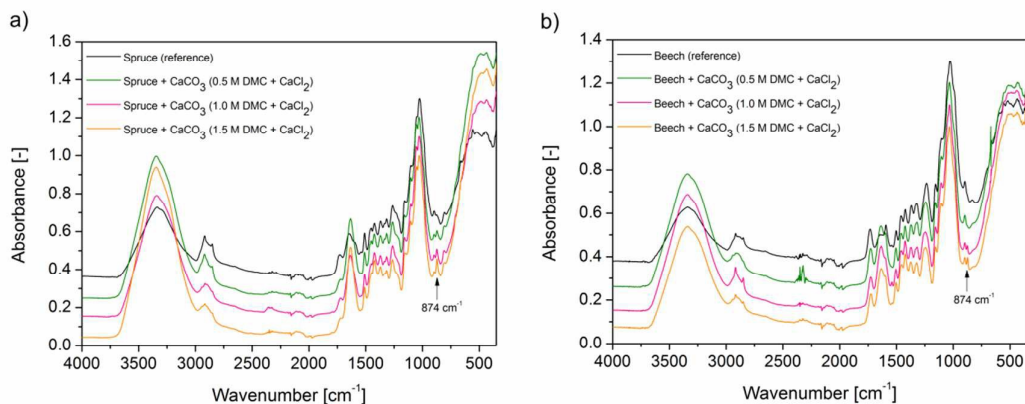
Figure S1. Typical Fourier-transform infrared spectra (FTIR) of pristine wood and CaCO$_3$/wood composites collected in the attenuated total reflection (ATR) mode: a) spruce b) beech. The ν$_2$ peak at 874 cm^{-1} shows the presence of calcite[2].

Raman microscopy
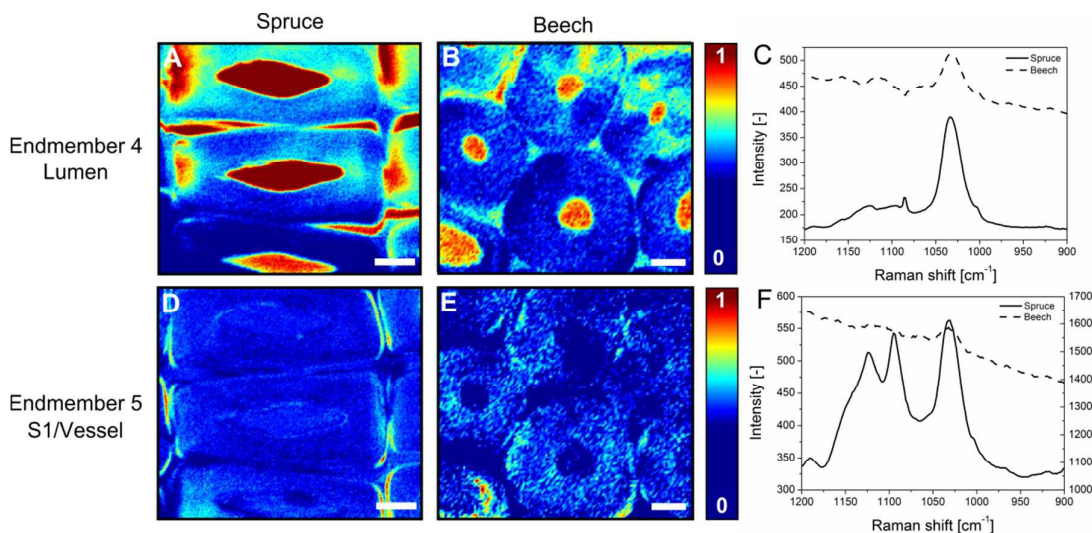
Figure S2. Raman mappings of CaCO$_3$/wood composites prepared at [DMC] = [CaCl$_2$] = 1.0 mol L^{-1} according to VCA analysis showing endmembers of spruce (A, D, solid line) and beech (B, E, dashed line) in the range |1200-900 cm^{-1}|. Endmember 4 (A, B, C): Lumen (1550-1640 cm^{-1}). Endmember 5 (D, E, F): S1 cell wall carbohydrates (1112 cm^{-1}, 1154 cm^{-1}) and beech vessel. C, F: Endmember spectra for spruce (solid line) and beech (dashed line). The left axis in F refers to spruce, the right axis to beech. Scale-bars in A and D correspond to 10 μm and in B and E to 5 μm, respectively.

Pyrolysis combustion flow calorimetry
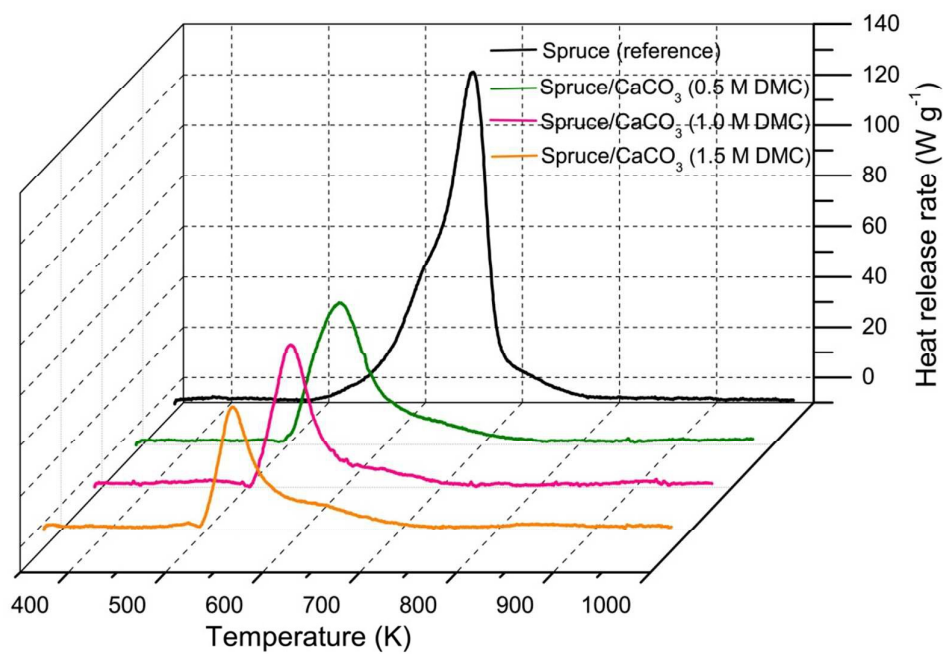
Figure S3. Pyrolysis combustion flow calorimetry: b) Typical temperature-dependent heat release rate curves of spruce samples after base-line correction.

3
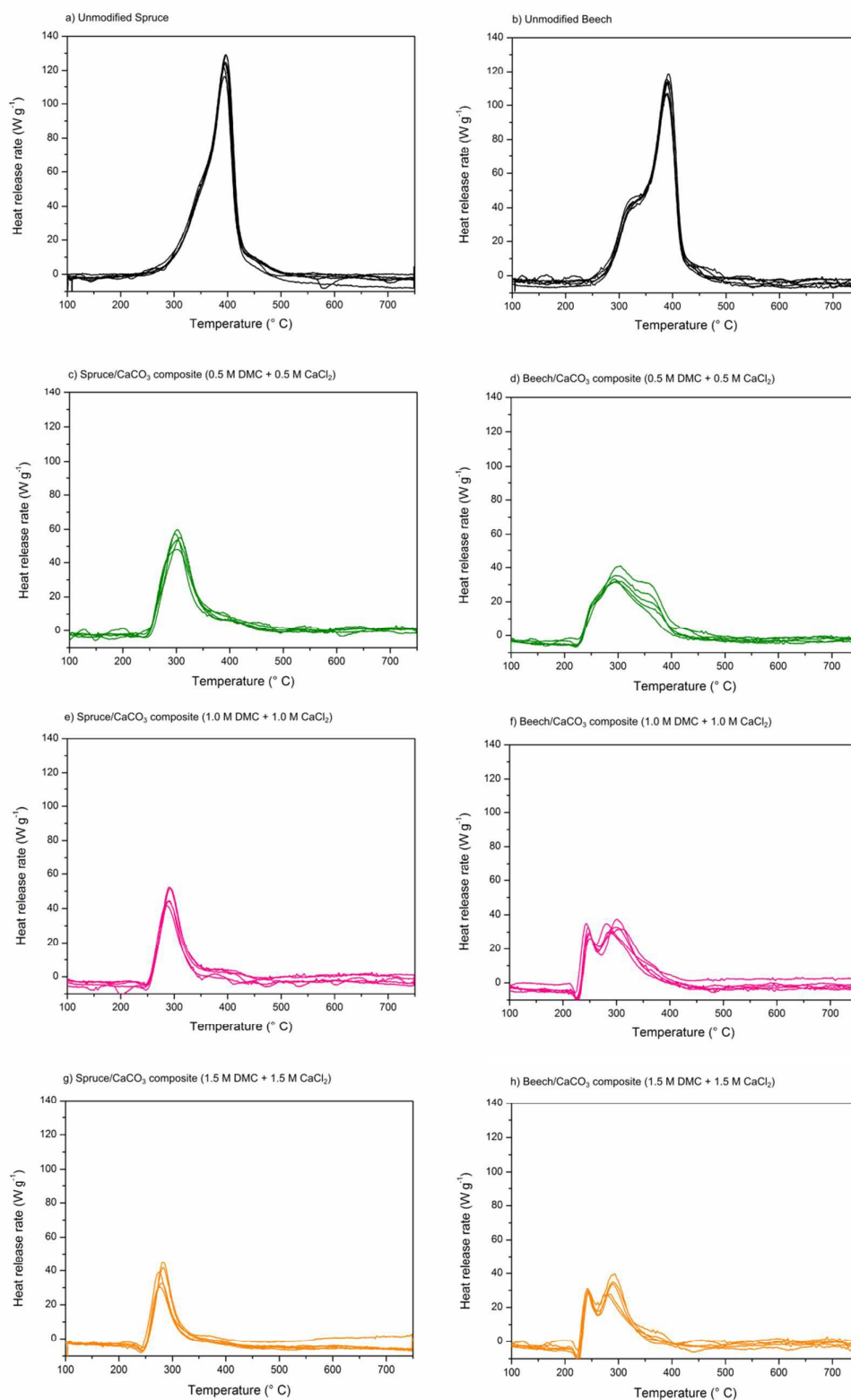
Figure S4. PCFC raw data: Temperature-dependent heat release rate curves of native wood and wood/CaCO$_3$ composites prepared from the release of CO$_2$ through a basic hydrolysis of dimethyl carbonate in the presence of calcium ions. a-d) Spruce. e-h) Beech.

4

Mass gain and equilibrium moisture of mineralized wood samples
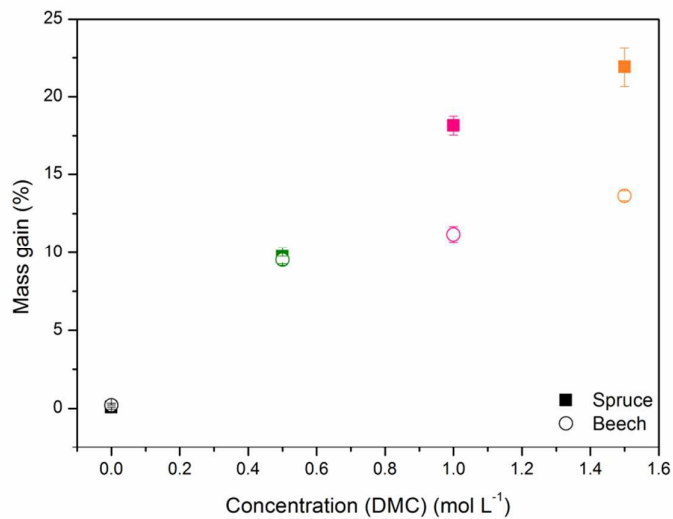
Figure S5. Mass gain of mineralized spruce and beech wood (10 mm edge length) prepared at different precursor concentrations [DMC] = [CaCl$_2$] in the dry state.
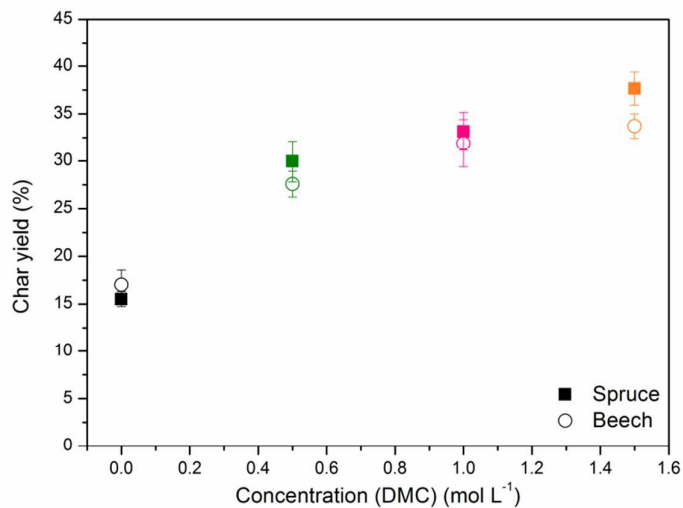
Figure S6. Char yield of native beech and spruce samples as a function of the precursor concentration [DMC] = [CaCl$_2$] calculated by weighing the test specimen before and after total combustion in pyrolysis combustion flow calorimetry.

5
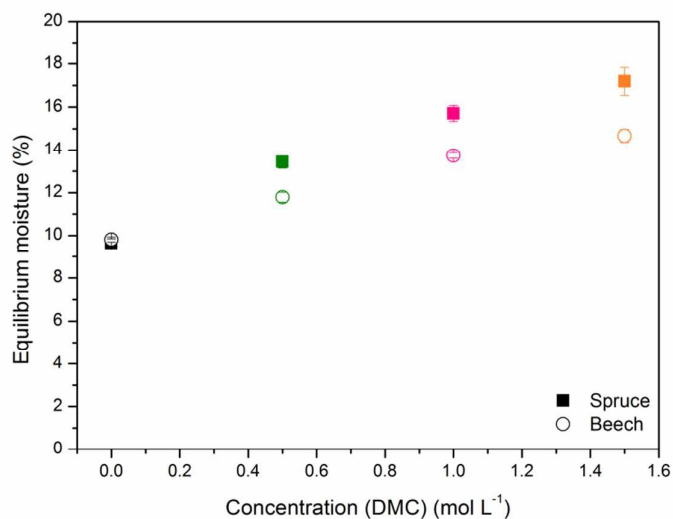
Figure S7. Equilibrium moisture of reference and mineralized wood as a function of the precursor concentration [DMC] = [CaCl$_2$] determined from the mass in the dry state (65° C) and at norm climate (65 % relative humidity, 20° C).

Thermogravimetric analysis

In addition to pyrolysis combustion flow calorimetry, thermogravimetric analysis gives complementary information on the mass loss in pure nitrogen at a constant heating rate. Below 100° C, the higher mass loss of the mineralized samples compared to the references (Figure S8-11) is attributed to their higher equilibrium moisture (see Figure S7). The first derivative allows to evaluate the slope of the TGA curve in the 100-500° C temperature range most relevant for wood combustion (Figure S9 and S11). Compared to the reference, the mineralisation treatment gives rise to a shift of the onset temperature to lower values and a decreased overall mass loss.
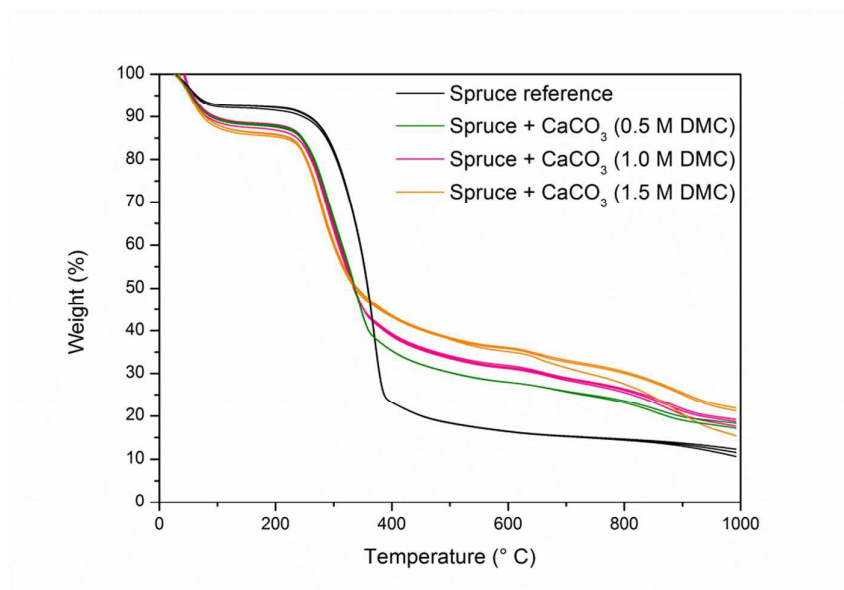
Figure S8. Thermogravimetric analysis of spruce composites in a temperature range 50-1000° C.
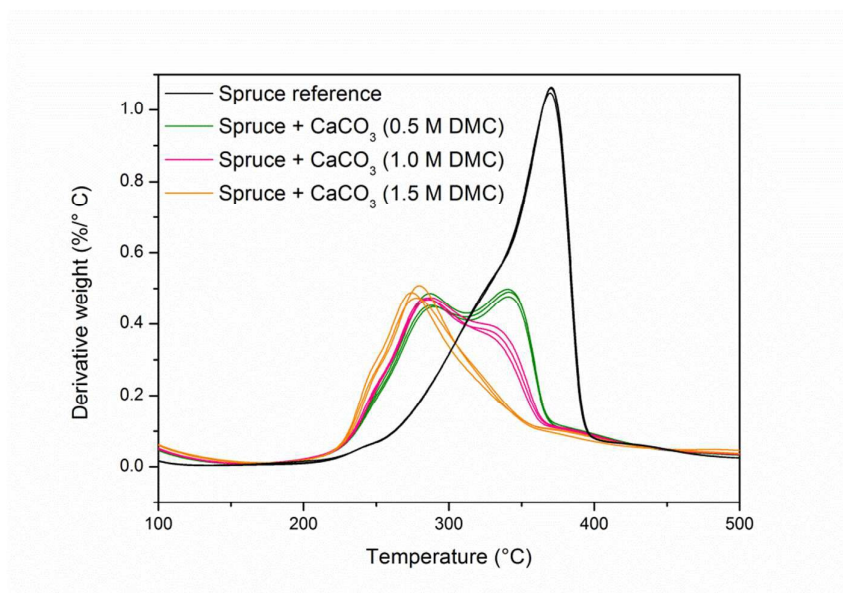
Figure S9. First derivative of thermogravimetrically determined mass of spruce composites in a temperature range 100-500° C.
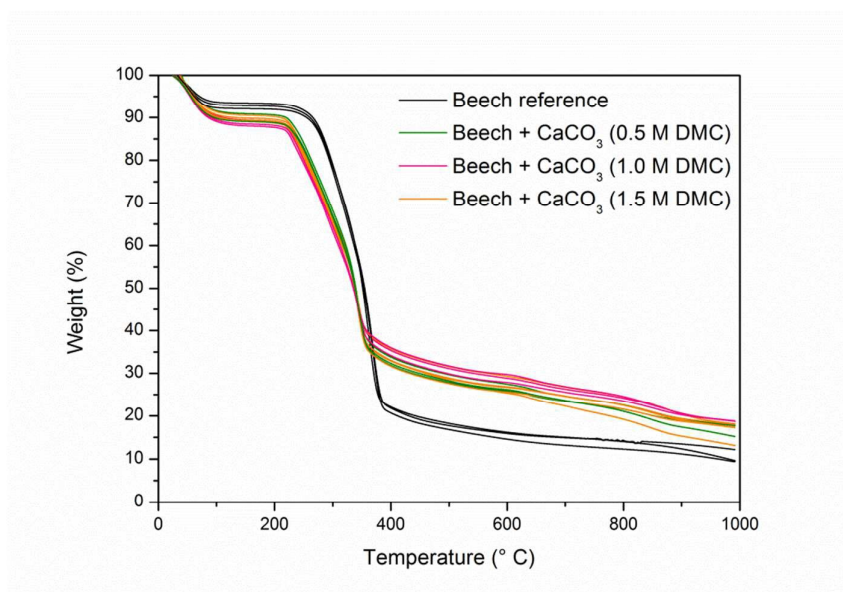
Figure S10. Thermogravimetric analysis of beech composites in a temperature range 50-1000° C.

7
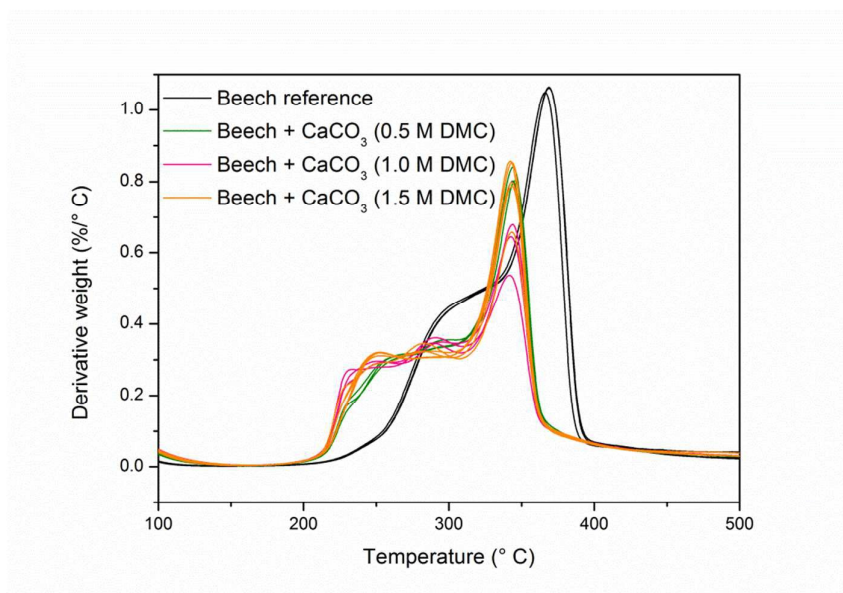
Figure S11. First derivative of thermogravimetrically determined mass of beech composites in a temperature range 100-500° C.

**Scanning electron microscopy and semi-quantitative energy-dispersive X-ray analysis**

Semi-quantitative energy-dispersive X-ray spectroscopy (SEM-EDX) of mineralized spruce and beech (precursor concentrations 1.5 M $CaCl_2$ and 1.5 M DMC) have been obtained in the center of an unwashed bulk specimen in 5 mm depth (Figure S12-15). It has to be taken into account that characteristic X-ray lines emerge from a bigger micron-ranged volume than the backscattered electrons in the SEM images. The relative elemental composition of the point analysis is given both in weight percentage (Wt%) and normalized atom percentage (At%). A comparison of the atom percentage of Na and Cl indicates that unreacted $CaCl_2$ is present apart from the reaction products NaCl and $CaCO_3$.
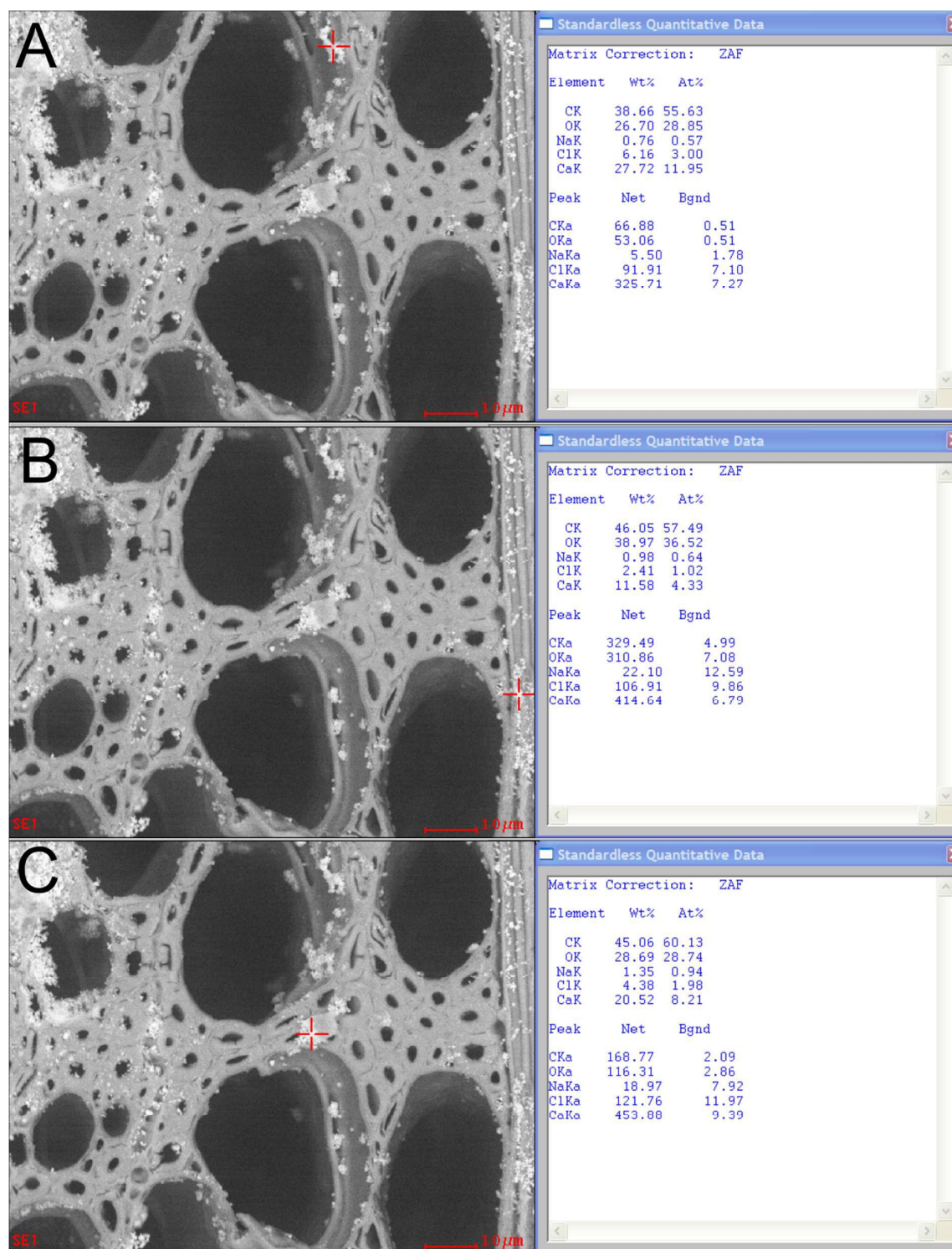
Figure S12A-C. SEM in the backscattered electron mode and semi-quantitative EDX analysis of CaCO$_3$/beech composites (non-washed, oven-dried at 65°C, conditioned to norm climate).

9
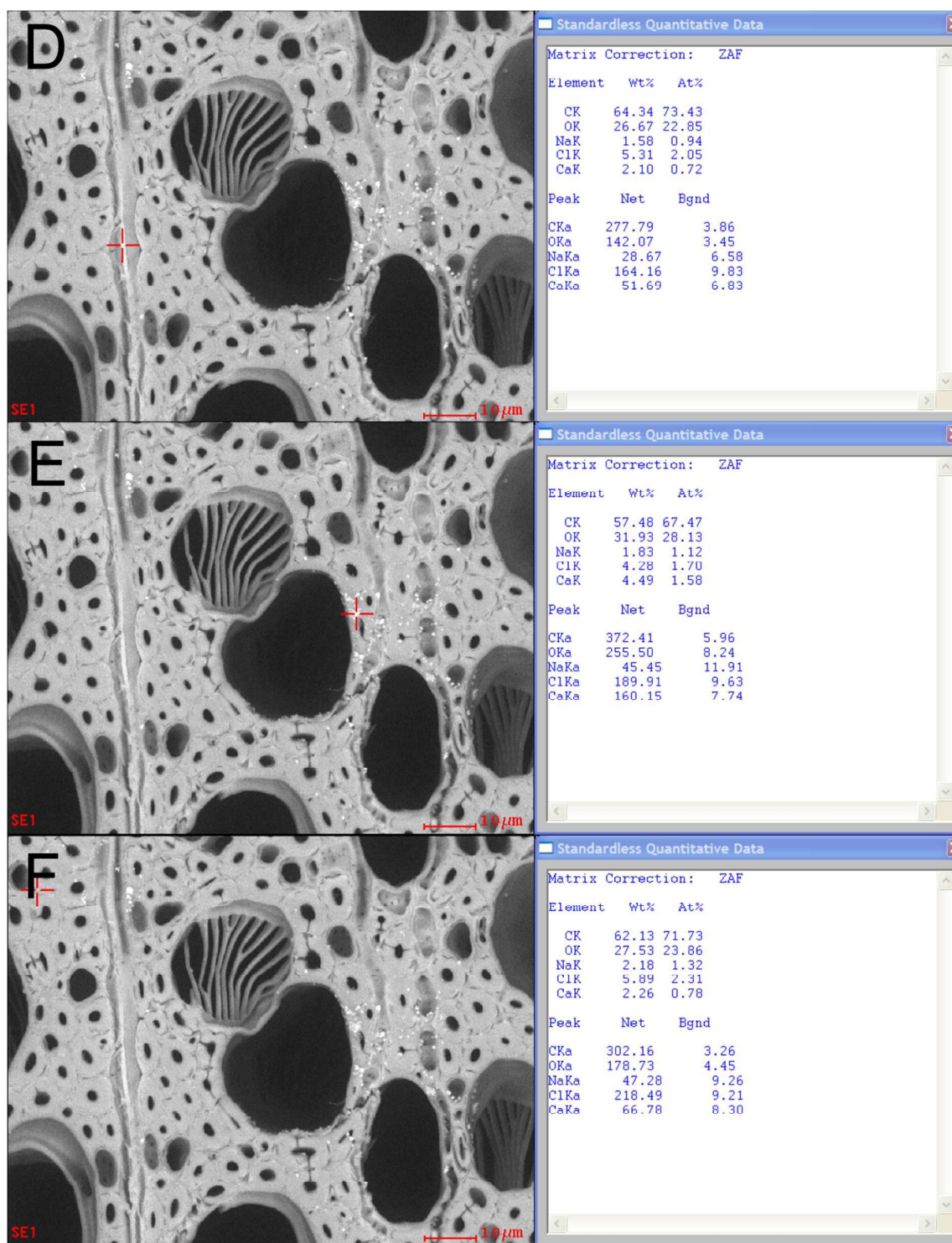
Figure S13D-F. SEM in the backscattered electron mode and semi-quantitative EDX analysis of CaCO$_3$/beech composites (non-washed, oven-dried at 65°C, conditioned to norm climate).

10
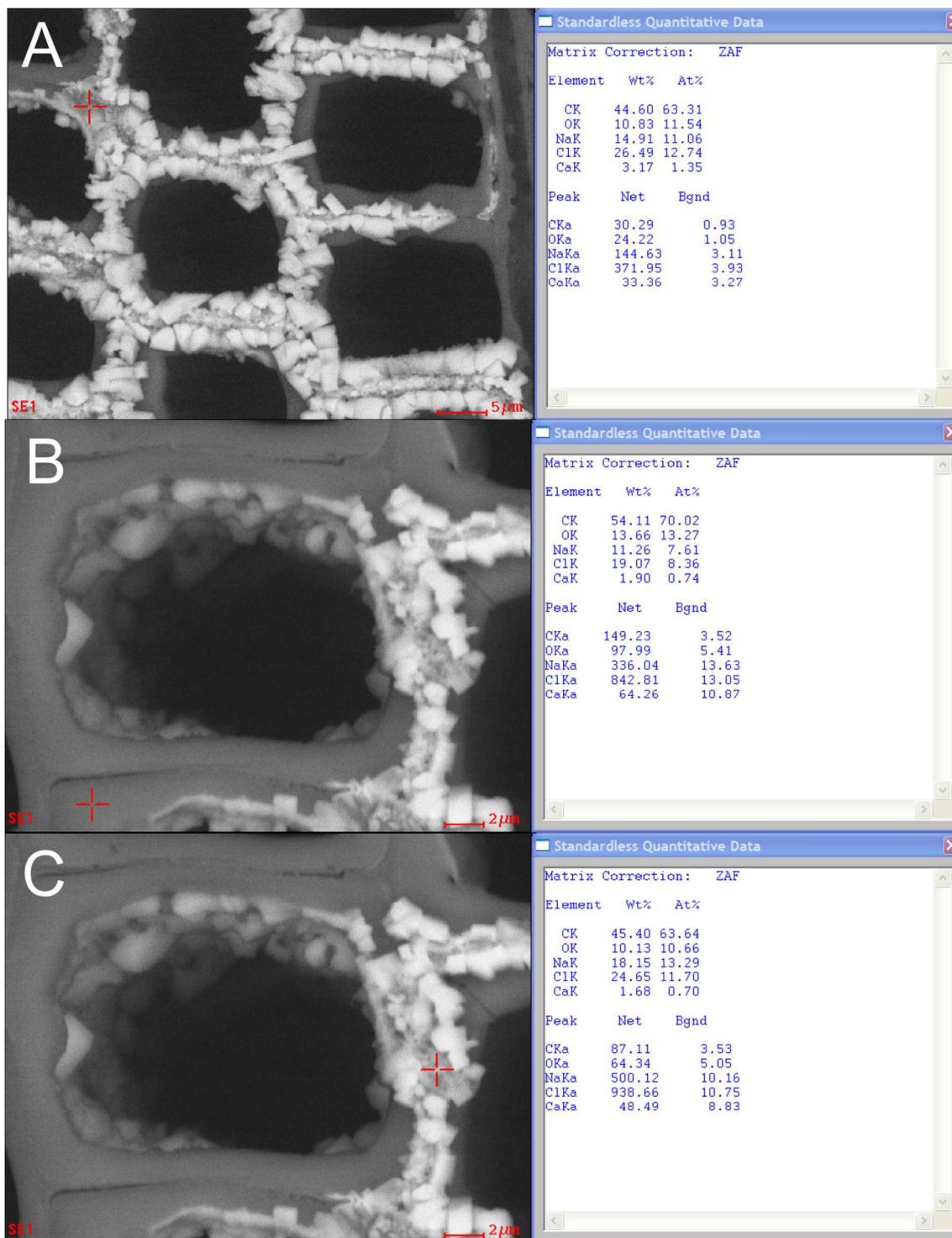
Figure S14A-C. SEM in the backscattered electron mode and semi-quantitative EDX analysis of CaCO$_3$/spruce composites (non-washed, oven-dried at 65°C, conditioned to norm climate).
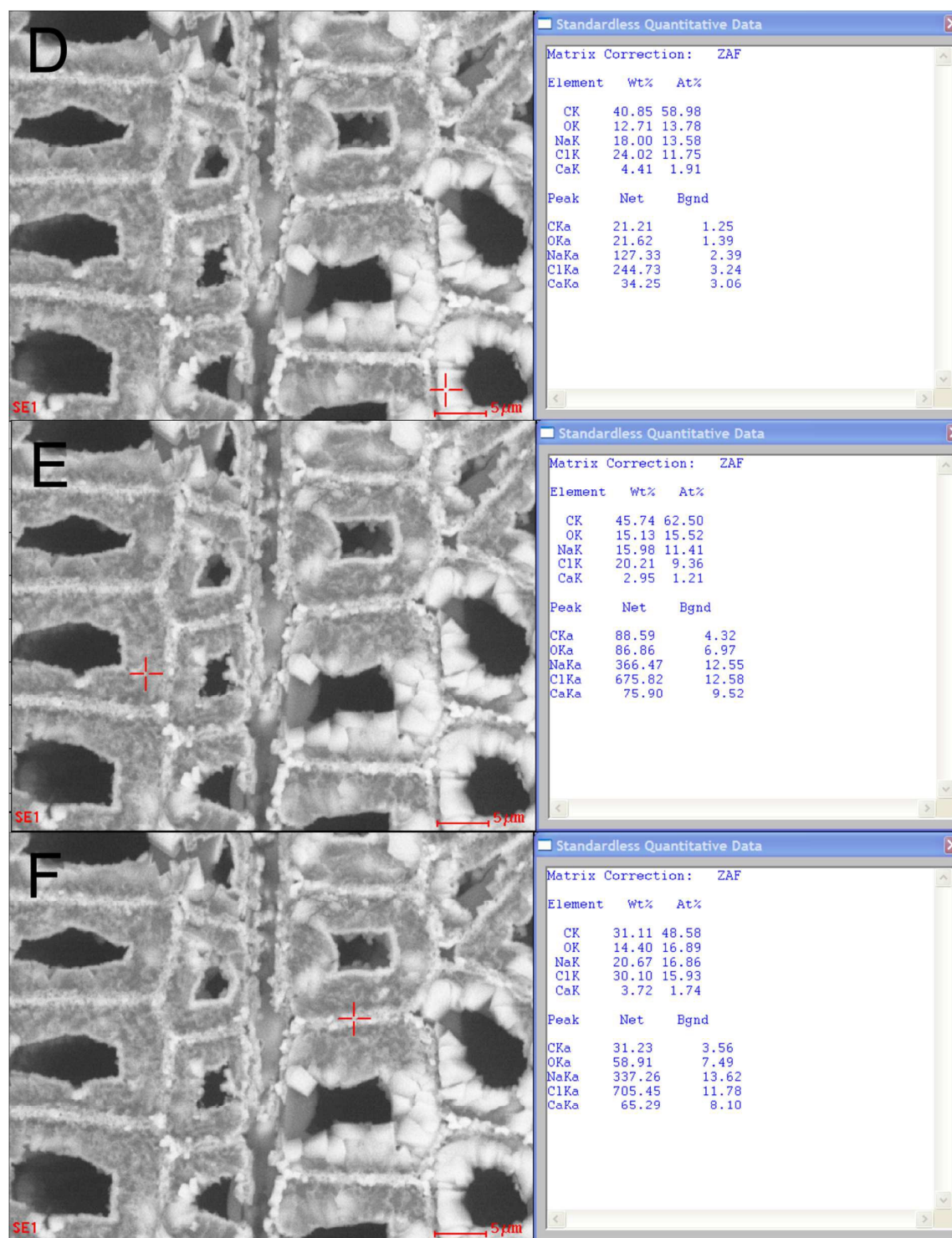
Figure S15D-F. SEM in the backscattered electron mode and semi-quantitative EDX analysis of CaCO₃/spruce composites (non-washed, oven-dried at 65°C, conditioned to norm climate).

X-ray powder diffraction

X-Ray powder diffraction of mineralized spruce without prior washing (Figure S16) demonstrates the formation of crystalline calcite $(CaCO_3)$[3] and sodium chloride $(NaCl)$[4] in the wood matrix, whereas the precursor salt calcium chloride

dihydrate (sinjarite) is not detected in the XRD spectrum[5]. We calculated the XRD pattern from Q values of $CaCl_2 \cdot 2H_2O$ reported in the literature[5] for a copper X-ray source ($\lambda_{CuK\alpha}$ = 1.541838 Å) yielding 2Θ = 64.3°, 44.1°, 40.6°, 38.5°, 36.0°, 33.7°, 32.2°, 30.7°, 30.2°, 28.6°, 26.5°, 25.2°, 24.2°, 23.6°, 22.9°, 21.5°, 20.9°, given as dotted lines in Figure S16. After washing the mineralized spruce for 3 h in slightly basic water, sodium chloride is removed according to XRD (Figure S17). Nevertheless, the presence of amorphous $CaCO_3$ in the sample cannot be ruled out. Amorphous calcium carbonate gives rise to a broad peak around $2\Theta \approx 40°$ [6]. A quantification of amorphous mineral phases in wood tissues, however, is highly challenging due to a background from amorphous cellulose domains (Figure S18). A detailed characterization of mineralized wood using X-ray techniques will be a subject of future investigations.
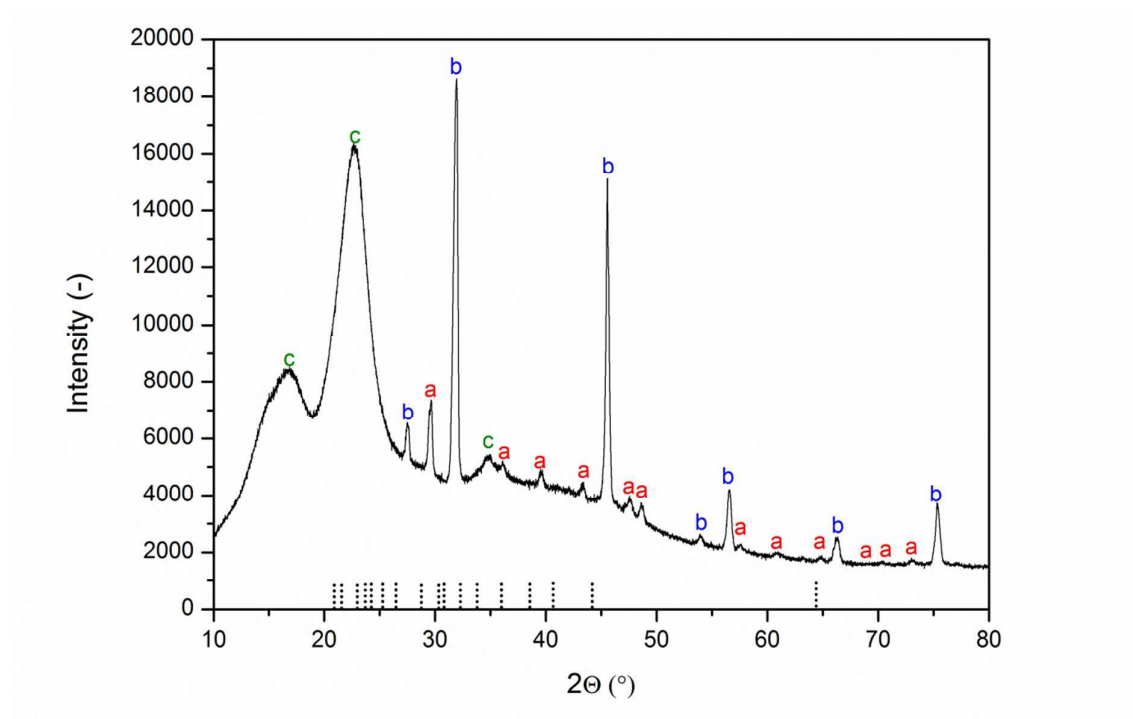
Figure S16. XRD of unwashed mineralized spruce showing crystalline portion of calcite (a), sodium chloride (b) and cellulose microfibrils (c). The dotted lines give the diffraction pattern of $CaCl_2 \cdot H_2O$ according to the literature[5].

13
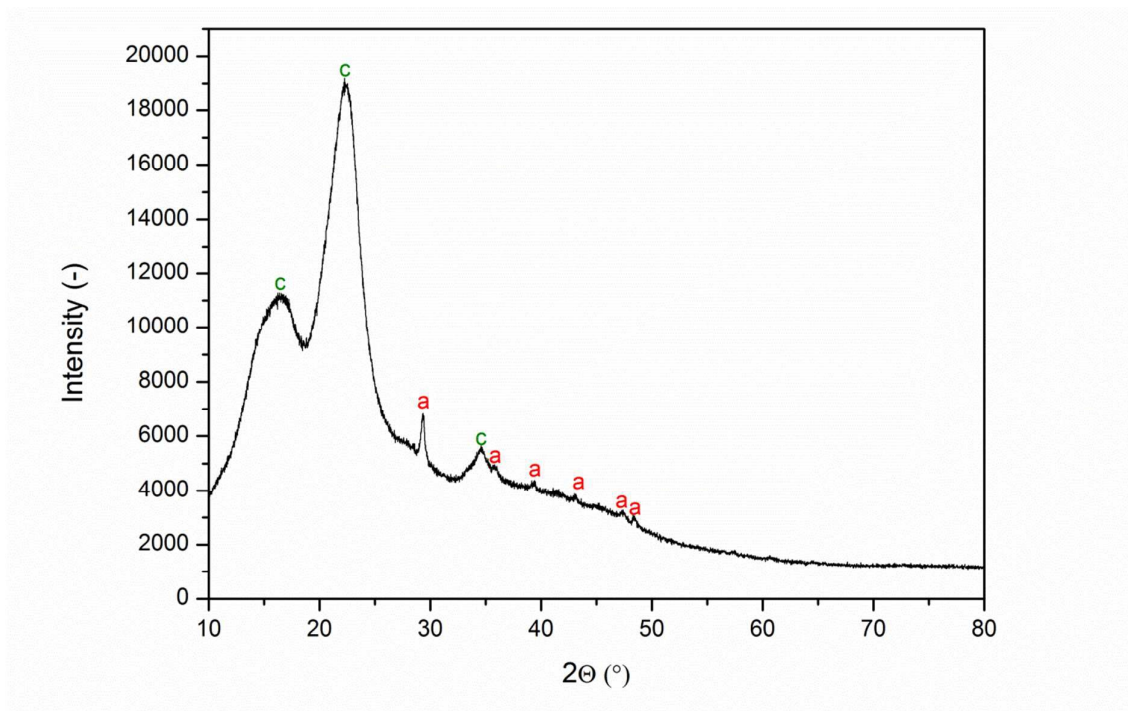
Figure S17. XRD of mineralized spruce washed in slightly basic water (pH ≈ 8) showing crystalline portion of calcite (a) and cellulose microfibrils (c).
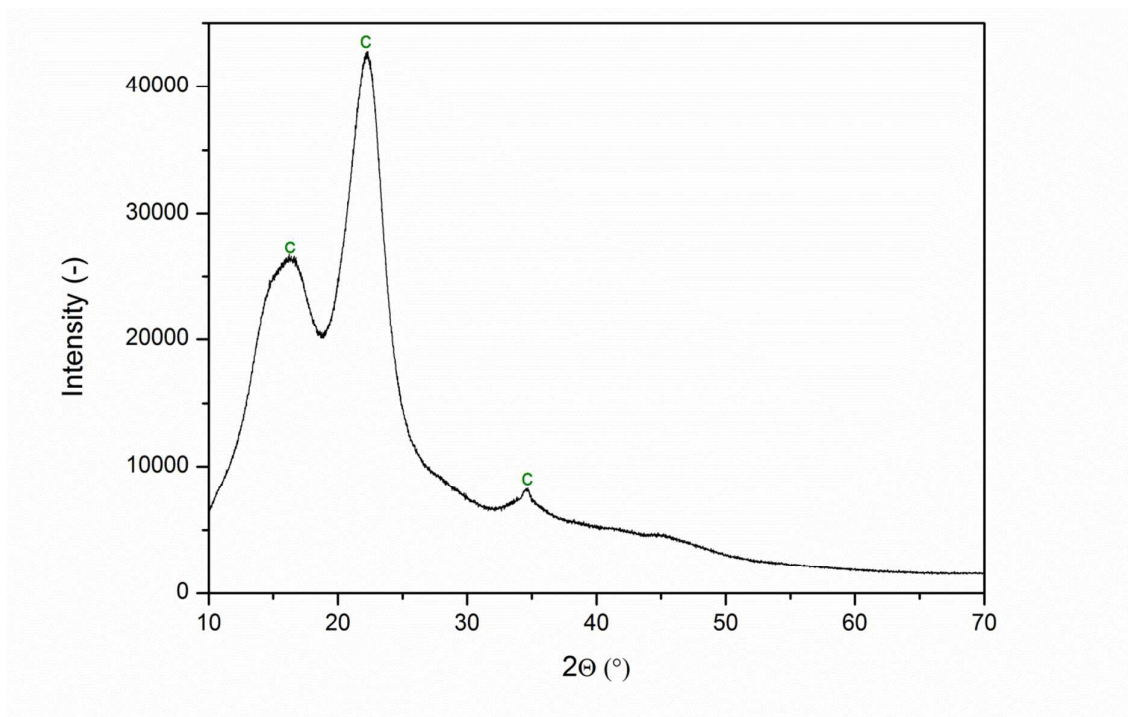

Figure S18. XRD of reference spruce showing cellulose microfibrils (c).

References

1.   Lyon, R. E.; Walters, R. N., Pyrolysis combustion flow calorimetry. *Journal of Analytical and Applied Pyrolysis* **2004,** *71* (1), 27-46.
2.   Andersen, F. A.; Brecevic, L., Infrared-spectra of amorphous and crystalline calcium carbonate. *Acta Chemica Scandinavica* **1991,** *45* (10), 1018-1024.
3.   Kontoyannis, C. G.; Vagenas, N. V., Calcium carbonate phase analysis using XRD and FT-Raman spectroscopy. *Analyst* **2000,** *125* (2), 251-255.
4.   Downs, R. T., The RRUFF Project: an integrated study of the chemistry, crystallography, Raman and infrared spectroscopy of minerals. In *Program and Abstracts of the 19th General Meeting of the International Mineralogical Association in Kobe*, Japan, **2006**; p Halite R070292.
5.   Aljubouri, Z. A.; Aldabbagh, S. M., Sinjarite, a new mineral from Iraq. *Mineralogical Magazine* **1980,** *43* (329), 643-645.
6.   Gorna, K.; Hund, M.; Vučak, M.; Gröhn, F.; Wegner, G., Amorphous calcium carbonate in form of spherical nanosized particles and its application as fillers for polymers. *Materials Science and Engineering: A* **2008,** *477* (1–2), 217-225.